frontiers | Frontiers in Earth Science

ORIGINAL RESEARCH
published: 06 July 2022
doi: 10.3389/feart.2022.927862

Multifractal Features of Particle-Size Distribution and Their Relationships With Soil Erosion Resistance Under Different Vegetation Types in Debris Flow Basin

Songyang Li[1,2†], Ruoyun Gao[1,2†], Maowei Huang[1], Liusheng Yang[1,2], Hang Yu[1,2], Chenhui Yu[1,2], Xue Tian[1,2], Jian Li[1,2] and Yongming Lin[1,2]*

[1]College of Forestry, Fujian Agriculture and Forestry University, Fuzhou, China, [2]Key Laboratory for Forest Ecosystem Process and Management of Fujian Province, Fuzhou, China

OPEN ACCESS

Edited by:
Haijun Qiu,
Northwest University, China

Reviewed by:
Songtang He,
Institute of Mountain Hazards and Environment CAS, China
Chao Ma,
Beijing Forestry University, China

***Correspondence:**
Yongming Lin
monkey1422@163.com

[†]These authors have contributed equally to this work and share first authorship

Specialty section:
This article was submitted to Geohazards and Georisks, a section of the journal Frontiers in Earth Science

Received: 25 April 2022
Accepted: 26 May 2022
Published: 06 July 2022

Citation:
Li S, Gao R, Huang M, Yang L, Yu H, Yu C, Tian X, Li J and Lin Y (2022) Multifractal Features of Particle-Size Distribution and Their Relationships With Soil Erosion Resistance Under Different Vegetation Types in Debris Flow Basin. Front. Earth Sci. 10:927862. doi: 10.3389/feart.2022.927862

Understanding the influence of vegetation types on soil particle-size distribution (PSD) is essential to evaluate the effects of sediment control by vegetation restoration. In this work, we studied the effects of different vegetation types, including bare land, meadow, shrub and forest on soil PSD in Jiangjiagou gully, Yunnan province, China. A total of 60 soil samples were collected and analyzed for soil particle size distribution using the laser diffraction method. Fractal theory was used to calculate multifractal parameters. The volume fraction of silt particles in shrub and forest is significantly higher than that in bare land, meadow, whereas the total volume fraction of sand particles in bare land and meadow exceed that in shrub and forest. The soil particle size distribution along soil layers has no significant difference in each vegetation type. The volumetric fractal dimension is significantly higher in forest and shrub than in bare land and grassland, but there is no significant difference between forest and shrub. In addition, soil erosion resistance exhibits significant differences of forest > shrub > grassland > bare land. Multifractal parameters are highest in bare land except for multifractal spectrum values ($f(\alpha_{max})$ and $f(\alpha_{min})$) and the maximum value of singularity index (α_{min}). All generalized dimensions spectra curves of the PSD are sigmoidal, whereas the singular spectrum function shows an asymmetric upward convex curve. Furthermore, soil erosion resistance has significant relationships with multifractal parameters. Our results suggest that multifractal parameters of the soil PSD can predict its anti-ability to erosion. This study also provides an important insight for the evaluation of soil structure improvement and the effects of erosion control by vegetation restoration in dry-hot valley areas.

Keywords: soil particle-size distribution, multifractal analysis, vegetation restoration, soil erosion resistance, debris flow-affected area

1 INTRODUCTION

Vegetation restoration is a key factor to control soil erosion in degraded land through both hydrological and mechanical mechanisms (Podwojewski et al., 2011; Burylo et al., 2012; Cui et al., 2019). It not only can reduce raindrop splash force, regulate surface runoff, and trap sediment (Lin et al., 2014), but also can promote soil erosion resistance (Gyssels et al., 2005; Descheemaeker et al., 2006; Ma et al., 2016; Deng et al., 2022). In general, the effect of vegetation on erosion control differs in vegetation types due to various plant coverage, species composition, and community structure (Lin et al., 2014; Dai et al., 2022). In detail, vegetation with highly complicated structure and layers has strong ability to prevent soil detachment and minimize soil movement (Lin et al., 2014), resulting in comparatively higher fine content and lower coarses particles (Burylo et al., 2012). However, many studies mainly focused on the relationship between vegetation change and the regulation and control of soil erosion (McVicar et al., 2010; Li et al., 2021a). The interaction between soil particle size distribution and vegetation types, especially in extremely degraded areas is poorly understood.

The particle-size distribution (PSD) is a typical property of soil texture and has significant effects on bulk density, porosity, organic matter, and cation exchange capacity (Bieganowski et al., 2013; Wang et al., 2019). Comparing the characteristics of soil PSD is essential to understand and determine the dynamics of soil structure induced by influence factors such as vegetation succession, tillage, reforestation, and grazing (Lyu et al., 2015; Yang et al., 2022). Soil PSD has an irregular shape and self-similar hierarchical structure, indicating that it has fractal features (Guan et al., 2011; Zhang et al., 2017). Therefore, soil PSD has been the focus of much research concerning on soil particle fractionation and physical processes (Peng et al., 2014; Lyu et al., 2015). Previous studies have focused on the effects of soil erosion on fractal dimension of soil PSD. For example, Liu et al. (2022) found that fractal dimension of soil PSD in hedgerows can reflect sediment reduction effect. Li et al. (2021a) showed that multifractal analysis captured the complexity of the PSD of suspend sediment in the Yangtze River. Although many findings with respect to fractal dimensions of soi PSD have been obtained, whether soil erosion anti-ability significantly respond to fractal dimensions of soil PSD is unknown.

In recent years, many studies have demonstrated that particle redistribution occurs in soil erosion process (Zhou et al., 2022; Liu et al., 2022; Zhang et al., 2020; Ma et al., 2021), this truth provides important clue that temporal changes in environmental conditions causing soil erosion can be identified (Schillereff et al., 2014; Wei et al., 2014). Therefore, the soil erosion resistance of different vegetation types could be reflected by their species diversity, plant density, and root characteristics (Jin and Chen, 2019; Xu et al., 2019). Several authors highlight that the size characteristics of eroded soil sediment contribute to the growing body knowledge on revised soil erosion model in the wake of erosion processes (Asadi et al., 2011; Shi et al., 2012; Liu et al., 2021). Hence, it is necessary to understand the relationship between soil erosion resistance and its PSD. However, recent works on soil PSD mostly concerned about stable or undisturbed ecosystems such as tidal flats (Lyu et al., 2015), forests (Wang et al., 2008; Xia et al., 2009), vegetation barriers (Bochet et al., 2000; Burylo et al., 2012), little is known about the relationship between soil erosion resistance of different vegetation types and fractal dimensions of soil PSD.

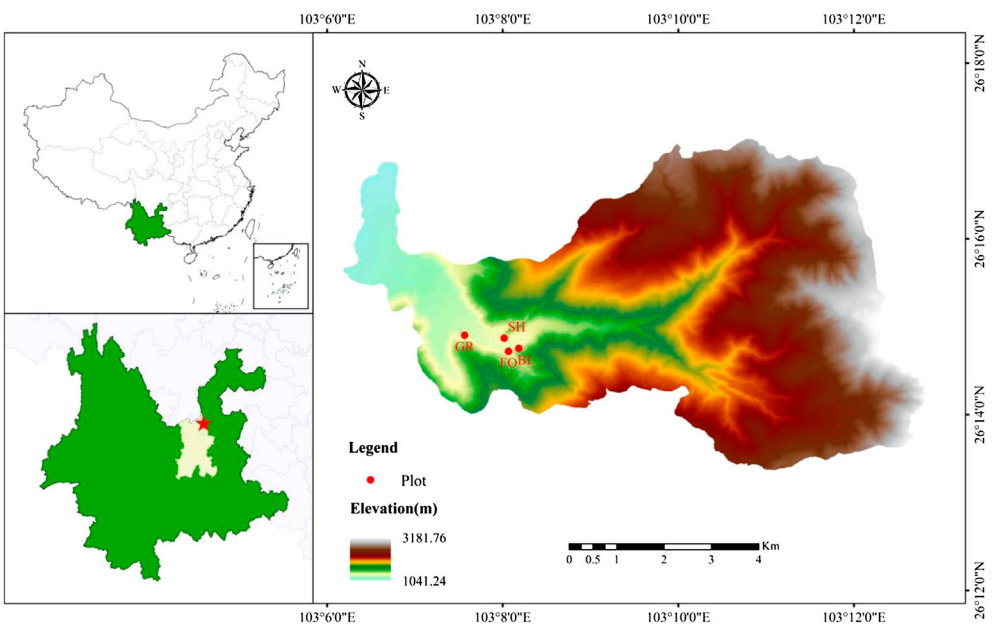

FIGURE 1 | Geographic location of the Jiangjiagou gully and four vegetation plots. BL: Bare land; GR: Grassland; SH: Shrub; FO: Forest.

TABLE 1 | Experimental conditions of four vegetation types.

Vegetation Types	Longitude/Latitude	Slope Gradient (o)	Slope-Aspect	Elevation (m)	Dominant Species	Vegetation Coverage (%)
Bare land	103°08′11″E/26°14′46″N	24	NE	1,356	—	5
Grassland	103°07′34″E/26°14′55″N	20	NE	1,288	*Heteropogon contortus*	40
Shrub	103°08′01″E/26°14′53″N	19	SW	1,337	*Desmodium racemosum*	80
Forest	103°08′04″E/26°14′44″N	20	NE	1,347	*Leucaena leucocephala*	90

FIGURE 2 | Field views of four vegetation plots.

In extremely degraded areas, fractal dimensions of soil PSD have been used to describe the degrees of soil damage, recovery phrase, and sediment retention ability (Deng et al., 2015; Cui et al., 2019; Luo et al., 2019). Singular fractal dimension of soil PSD can vary in response to major earthquakes and can predict the effects of earthquake disturbance on soil system (Deng et al., 2015). Soil PSD-based analyses also can reflect recover phrase when natural restoration occurred in disaster-affected areas (Luo et al., 2019). Furthermore, fractal dimension of sediment PSD can reveal sediment retention ability of plants (Cui et al., 2019). In our study area—dry-hot valley of Jinsha River, there also was some research on the relationship between fractal dimensions of soil PSD and soil properties (Xie and Wei, 2011; Li et al., 2021c; Chen et al., 2016), but little research has been done to understand the effects of soil sediment sorting by different vegetation types and the relationship between soil erosion resistance and fractal dimensions of soil PSD except some qualitative analyses or overall trend analyses (Wang et al., 2004; Cui et al., 2005).

In this study, we sought to estimate the impacts of vegetation types on the soil PSD characteristics using a typical basin of dry-hot valley—Jiangjiagou gully as a case study. Our objectives are to 1) reveal the soil PSD in typical debris flow basin using both singular and multi-fractal analysis; 2) to determine whether fractal dimensions reflect the change of vegetation types; and 3) to identify the influence of multifractal parameters on the soil erosion resistance. Our work took an integrative approach to study the effects of vegetation types on soil PSD and the relationship between soil erosion resistance and fractal dimensions of soil PSD. This study could provide theoretical support for ecological restoration and vegetation community improvement and help identify ways to rapidly evaluate the effects of soil sediment sorting and erosion control by vegetation types in dry-hot valley.

2 STUDY AREA

The study area is the Jiangjiagou watershed, Dongchuan district, Kunming, Yunnan province, China (latitude 26°13′–26°17′ N, longitude 103°6′–103°13′ E). It is in the altitude between 1,042 and 3269 m m s L. (**Figure 1**). The study area has three vertical climate types including 1) dry-hot valley with an elevation ranging from 1,042 to 1600 m, annual precipitation of 600–700 mm year^{-1}, mean annual temperature of 20°C, and

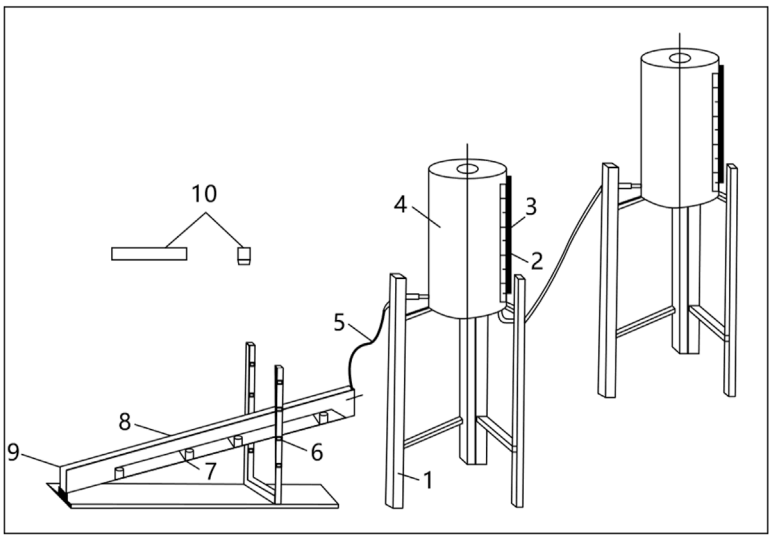

FIGURE 3 | Schematic diagram of anti-scouring test equipment (Chen et al., 2014). 1 is a bucket rack; 2 is a scale ruler; 3 is a glass tube; 4 is a bucket; 5 is a water pipe; 6 is a still water chamber; 7 is a skid; 8 is the flume for the test; 9 is the site for putting the samples; 10 is the cutting ring with 200 cm^3 (10 cm length, 5 cm width, and 4 cm height).

average annual potential evapotranspiration of 3,700 mm $year^{-1}$; 2) subtropical and sub-humid warm temperate climate with an elevation ranging from 1,600 to 2200 m, annual precipitation of 700–850 mm $year^{-1}$, mean annual temperature of 13°C, and average annual potential evapotranspiration of about 1700 mm $year^{-1}$; 3) humid warm temperate climate with an elevation ranging from 2200 to 3269 m, annual precipitation of about 1,200 mm $year^{-1}$, mean annual temperature of 7°C, and average annual potential evapotranspiration of about 1,350 mm $year^{-1}$. The main soil types in dry-hot valley are calcic vertisols and calcic regosols according to the WRB system (Li et al., 2021b).

Due to severe soil and water loss, viscous debris flows have occurred frequently in Jiangjiagou Gully since the early Late Pleistocene. They combined with human deforestation to destroy vegetation during the period of 1950–1970, resulting in serious ecological degradation and native vegetation destruction (Lin et al., 2014). Hence, original vegetation has been replaced by man-made forests. At present, in dry-hot valley of Jiangjiagou gully, *Leucaena leucocephala* and *Eucalyptus camaldulensis* were planted as the main man-made forests; Shrubs were mainly dominated by *Coriaria sinica*, *Salix myrtillacea*, *Desmodium racemosum*, and *Sophora davidii*; Grasslands were mainly dominated by *Heteropogon contortus*, *Eulaliopsis binata*, and *Themeda triandra*. However, vegetation coverage occupied <10% of the total area of dry-hot valley in 2004 (Cui et al., 2005). Therefore, various vegetation types enable Jiangjiagou gully to be an ideal site for studying the relationship between the soil erosion resistance of vegetation types and fractal dimensions of soil PSD.

Though the average hillslope is 43°in Jiangjiagou watershed (Lin et al., 2014), forests are mainly on slopes <25°. To avoid the discrepancy in different slope gradients, four vegetation plots were selected, including bare land, grassland, shrub, forest in Jiangjiagou gully (**Table 1**). All four experimental plots developed from landslide mass (<40 years) with the soil type of calcic regosols are located in the downstream of the Jiangjiagou gully near to Dongchuan Debris Flow Observation and Research Station, Chinese Academy of Sciences (**Figure 2**). Among four plots, bare land developed under natural conditions with slope gradient of 24°and northeast facing slope. Grassland developed from bare land to *Heteropogon contortus* grassland with slope gradient of 20°and northeast facing slope. Shrub developed from bare land to *Desmodium racemosum* shrub with slope gradient of 19°and southwest facing slope. Forest was reforested without land leveling projects in 2004 with *Leucaena leucocephala*, slope gradient of 20°and northeast facing slope.

3 MATERIALS AND METHODS

3.1 Soil Sampling and Analysis

We set up three random quadrats (10 × 10 m in forest, 5 × 5 m in shrub, and 1 × 1 m in both grassland and bare land) each vegetation type. In selected quadrat, five soil samples were collected from the depths of 0–10 cm, 10–20 cm, 20–30 cm, 30–40 cm, and 40–50 cm. In addition, one sample was taken with a standard 200 cm^3 volume (10 cm length, 5 cm width, and 4 cm height) from each soil depth for determining soil erosion resistance. A total of 60 soil samples for soil particles and soil erosion resistance were collected from the four vegetation types.

The portion to be analyzed for soil particles were taken to the lab, air-dried, disaggregated, and passed through 2 mm screen. We used the Longbench Mastersizer 2000 laser particle size analyzer to analyze the fractions particle with size <2 mm (Li et al., 2021a). The 10 ml 10% H_2O_2 was used to remove organic

matter to soak each 0.3 g soil sample for 24 h. Each sample was then treated with 5 ml of 10% HCl for 10 min to eliminate carbonate salts. Deionized water was added up to 500 ml to rinse the residual H_2O_2 and HCl for 12 h before the liquid supernatant was removed, until the pH of sample solution was adjusted to 7. We added 5 ml 0.1 ml/L sodium hexametaphosphate to separate soil particles before measurement and used the laser particle analyzer to measure the percentage volume of soil particles in the range 0.02–2000 μm after ultrasonic vibration for 10 min.

The portion to be analyzed for soil erosion resistance was stored in a plastic bag to avoid desiccation. We used the anti-scouring test equipment (**Figure 3**) and the method described by Chen et al. (2014) to determine soil erosion resistance:

$$k = q \times t/m \tag{1}$$

where k is the soil erosion resistance (Ls/g); q is the water volume used in flume experiment (L); t is the experiment time (s); m is the sediment weight eroded by water.

3.2 Fractal Models

The traditional approach for fractal characteristics of soil PSD is using unitedly laser diffraction method and fractal analysis (Tyler and Wheatcraft, 1992; Su et al., 2004; Peng et al., 2014; Lyu et al., 2015). Presently, two common methods including singular and multi-fractal analysis are widely used (Lyu et al., 2015). Singular fractal analysis can describe the overall or average characteristics of soil PSD and predict the change of related soil properties (Guan et al., 2011; Li et al., 2019), but seldom clearly understand the local heterogeneity of soil PSD. Therefore, multifractal analysis is used to determine the intrinsic variability of soil PSD in more detail (Lyu et al., 2015).

3.2.1 Volumetric Fractal Dimension

According to the frequency histogram obtained from the Longbench Mastersizer 2000 laser particle size analyzer, we used volumetric fractal model to establish the granularity of the soil particles as follows (Wang et al., 2005; Li et al., 2021b):

$$\frac{V_{(r<R)}}{V_T} = \left(\frac{R}{\lambda_v}\right)^{3-D_v} \tag{2}$$

where R is the soil particle size in mm; $V_{(r<R)}$ is the cumulative volume percent of particles lower than R; V_T is the total volume of soil particles; λ_V is the maximum particle size in mm; and D_v is the volumetric fractal dimension of the soil PSD. The value of R was the arithmetic mean of the lower and upper limits of a certain class.

The following logarithmic expression was derived from **Eq. 2**:

$$\log\left[\frac{V_{(r<R)}}{V_T}\right] = (3 - D_v)\log\left(\frac{R}{\lambda_v}\right) \tag{3}$$

using **Eq. 3**, the D_v value is equal to three minus the slope of the logarithmic linear regression equation, representing the space-filling efficiency of particles (Perfect & Kay, 1995; Biswas, 2019).

3.2.2 Calculation of the Multifractal Parameters

In this study, the measurement interval I = [0.02, 2000] of the laser particle size analyzer is divided into 64 smaller intervals $I_i = [\varphi_i, \varphi_{i+1}]$, $I = 1, 2 \ldots, 64$, with constant lg $(\varphi_{i+1}/\varphi_i)$. A new dimensionless interval $J = [0, 5.3]$ can then be created. A number $N(\varepsilon) = 2^k$ of cells with equal size $\varepsilon = 5.3 \times 2^{-k}$ for k is set up ranging from 1 to 5 (i.e., ε= 2.65, 1.325, 0.6625, 0.33125, and 0.165625). We created a certain measure μ that distributes over the interval of sizes I and each cell $\mu_i(\varepsilon)$ is contained in available data. $N(\varepsilon)$ is taken as the number of samples when the scale is ε; and $\mu_i(\varepsilon)$ is the probability density (percentile) of the ith subinterval (J_i), namely the sum of all measurements in the sub interval J_i. The generalized fractal dimension D_q is defined as follows:

$$D_q = \lim_{\varepsilon\to 0} \frac{1}{q-1} \frac{\lg\left[\sum_{i=1}^{N(\varepsilon)} \mu_i(\varepsilon)^q\right]}{lg\varepsilon} \quad (q \neq 1) \tag{4}$$

$$D_1 = \lim_{\varepsilon\to 0} \frac{\sum_{i=1}^{N(\varepsilon)} \mu_i(\varepsilon) \lg \mu_i(\varepsilon)}{lg\varepsilon} \quad (q = 1) \tag{5}$$

The singularity spectrum could be computed through a parameter q by:

$$\alpha(q) = \lim_{\varepsilon\to 0} \frac{\sum_{i=1}^{N(\varepsilon)} \mu_i(q,\varepsilon) \lg \mu_i(\varepsilon)}{\lg\varepsilon} \tag{6}$$

$$f(\alpha) = \lim_{\varepsilon\to 0} \frac{\sum_{i=1}^{N(\varepsilon)} \mu_i(q,\varepsilon) \lg \mu_i(q,\varepsilon)}{\lg\varepsilon} \tag{7}$$

using **Eqs 4–7**), in the range of $-10 \le q \le 10$, the fitting calculation is carried out with 1 step size to get $D(q)$, $\alpha(q)$ and $f(\alpha)$. When q = 0, D_0 is the capacity dimension, reflecting the range of a continuous distribution. When q = 1, D_1 is the entropy dimension of the measure, providing a measure of the heterogeneity of soil particle size distribution. When q = 2, D_2 is the correlation dimension that can capture some of the inner details of the particle-size distributions. The parameter of D_1/D_0 can be used to quantitatively describe the dispersion degree of soil particle size distribution (Guan et al., 2011; Rodríguez-Lado & Lado, 2017).

The parameters of $\alpha(q)$ and $f(\alpha)$ can characterize local multifractal characteristics of soil particle size distribution. $\alpha(0)$ is the average value of multifractal singular spectrum. The greater $\alpha(0)$ means the smaller the local density of soil particle size distribution.

The width of multifractal singular spectrum $\Delta\alpha(q)$ representing the spatial heterogeneity of soil particle size distribution is defined as follow:

$$\Delta\alpha(q) = \alpha(q)_{\max} - \alpha(q)_{\min} \tag{8}$$

where the min and max denote the minimum and maximum values, respectively.

The shape of multifractal singular spectrum Δf [$\alpha(q)$] is defined as follow:

$$\Delta f[\alpha(q)] = f\left[\alpha(q)_{\max}\right] - f\left[\alpha(q)_{\min}\right] \tag{9}$$

TABLE 2 | Soil particle size distribution and singular fractal dimension among four vegetation types and five soil layers. BL: Bare land; GR: Grassland; SH: Shrub; FO: Forest; *D*: volumetric fractal dimension; SER: Soil erosion resistance; Different letters indicate significant differences at $p < 0.05$. All data are shown using mean ± standard error. * means median; † means mode.

Source	Very Coarse Sand (1,2 mm)	Coarse Sand (0.5–1 mm)	Medium Sand (0.25–0.5 mm)	Fine Sand (0.1–0.25 mm)	Very Fine Sand (0.05–0.1 mm)	Silt (0.002–0.05 mm)	Clay (< 0.002 mm)	*D*	SER
Vegetation types (VT)	BL (n = 15)0.25 ± 0.37^{a}	7.41 ± 4.01^{a}	19.04 ± 5.03^{a}	11.53 ± 2.12^{a}	12.40 ± 2.95^{a}	42.76 ± 7.08^{b}	6.51 ± 0.86^{c}	2.63 ± 0.02^{c}	21.32 ± 5.17^{a}
	*0.06 †0	*7.78 †Null	*20.53 †Null	*11.26 †Null	*11.55 †Null	*43.39 †Null	*6.47 †Null	*2.63 †Null	*22.05 †Null
	GR (n = 15)0.13 ± 0.41^{a}	4.12 ± 3.66^{b}	16.14 ± 4.54^{a}	12.82 ± 3.06^{a}	12.70 ± 1.69^{a}	46.06 ± 7.37^{b}	7.99 ± 0.87^{c}	2.65 ± 0.02^{b}	44.02 ± 4.34^{b}
	*0 †0	*3.30 †Null	*15.39 †Null	*11.80 †Null	*12.45 †Null	*45.69 †Null	*7.78 †Null	*2.65 †Null	*42.66 †Null
	SH(n = 15)0^{a}	0.51 ± 1.10^{c}	4.94 ± 4.26^{b}	7.00 ± 2.28^{b}	9.49 ± 1.43^{b}	67.61 ± 6.28^{a}	10.46 ± 1.10^{b}	2.70 ± 0.02^{a}	83.71 ± 8.95^{c}
	*0 †0	*0.02 †Null	*3.53 †Null	*7.39 †Null	*9.75 †Null	*68.76 †Null	*10.86 †Null	*2.71 †Null	*82.48 †Null
	FO(n = 15)0.00 ± 0.00^{a}	0.71 ± 1.60^{c}	6.06 ± 8.47^{b}	6.26 ± 6.12^{b}	7.73 ± 2.44^{b}	66.68 ± 14.38^{a}	12.58 ± 2.68^{a}	2.72 ± 0.04^{a}	92.10 ± 12.17^{days}
	*0 †0	*0.20 †Null	*2.13 †Null	*3.63 †Null	*7.16 †Null	*72.11 †Null	*13.83 †Null	*2.74 †Null	*90.72 †Null
	p = 0.051	$p < 0.001$	$p < 0.001$	$p < 0.001$	$p < 0.001$	$p < 0.001$	$p < 0.001$	$p < 0.001$	$p < 0.001$
Soil layers (SL)	0–10 cm (n = 12)0.01 ± 0.04^{a}	2.16 ± 2.79^{a}	10.58 ± 7.23^{a}	9.03 ± 4.40^{a}	11.41 ± 4.51^{a}	57.46 ± 12.74^{a}	9.39 ± 2.59^{a}	2.68 ± 0.04^{a}	58.04 ± 32.65^{a}
	*0 †Null	*0.74 †Null	*9.28 †Null	*9.52 †Null	*11.33 †Null	*53.35 †Null	*8.43 †Null	*2.66 †Null	*61.02 †Null
	10–20 cm (n = 12)0.11 ± 0.29^{a}	3.40 ± 4.05^{a}	10.88 ± 8.52^{a}	8.61 ± 4.39^{a}	10.21 ± 3.09^{a}	57.44 ± 15.10^{a}	9.34 ± 2.77^{a}	2.68 ± 0.04^{a}	68.94 ± 36.81^{a}
	*0 †Null	*1.24 †Null	*12.17 †Null	*9.28 †Null	*11.08 †Null	*51.91 †Null	*8.19 †Null	*2.65 †Null	*72.58 †Null
	20–30 cm (n = 12)0.22 ± 0.51^{a}	4.51 ± 4.84^{a}	13.64 ± 10.12^{a}	9.51 ± 5.09^{a}	10.08 ± 2.08^{a}	52.87 ± 16.84^{a}	9.12 ± 3.29^{a}	2.67 ± 0.05^{a}	58.72 ± 26.57^{a}
	*0 †Null	*2.52 †Null	*15.16 †Null	*9.61 †Null	*10.88 †Null	*49.45 †Null	*7.95 †Null	*2.66 †Null	*58.31 †Null
	30–40 cm (n = 12)0.02 ± 0.04^{a}	2.69 ± 3.48^{a}	11.40 ± 8.33^{a}	10.17 ± 4.61^{a}	10.46 ± 1.76^{a}	55.47 ± 14.67^{a}	9.65 ± 2.60^{a}	2.68 ± 0.05^{a}	62.81 ± 30.24^{a}
	*0 †Null	*0.57 †Null	*11.04 †Null	*10.23 †Null	*9.97 †Null	*58.06 †Null	*10.06 †Null	*2.69 †Null	*76.24 †Null
	40–50 cm (n = 12)0.10 ± 0.23^{a}	2.78 ± 4.56^{a}	10.58 ± 8.61^{a}	9.57 ± 5.39^{a}	10.57 ± 3.00^{a}	56.70 ± 15.92^{a}	9.67 ± 3.09^{a}	2.68 ± 0.05^{a}	56.42 ± 26.38^{a}
	*0 †Null	*0.25 †Null	*9.66 †Null	*8.57 †Null	*11.10 †Null	*57.99 †Null	*9.15 †Null	*2.68 †Null	*62.34 †Null
	p = 0.412	p = 0.667	p = 0.898	p = 0.951	p = 0.846	p = 0.941	p = 0.990	p = 0.975	p = 0.864
VT×SL	p = 0.783	p = 0.185	p = 0.784	p = 0.813	p = 0.644	p = 0.901	p = 0.858	p = 0.829	p = 0.025

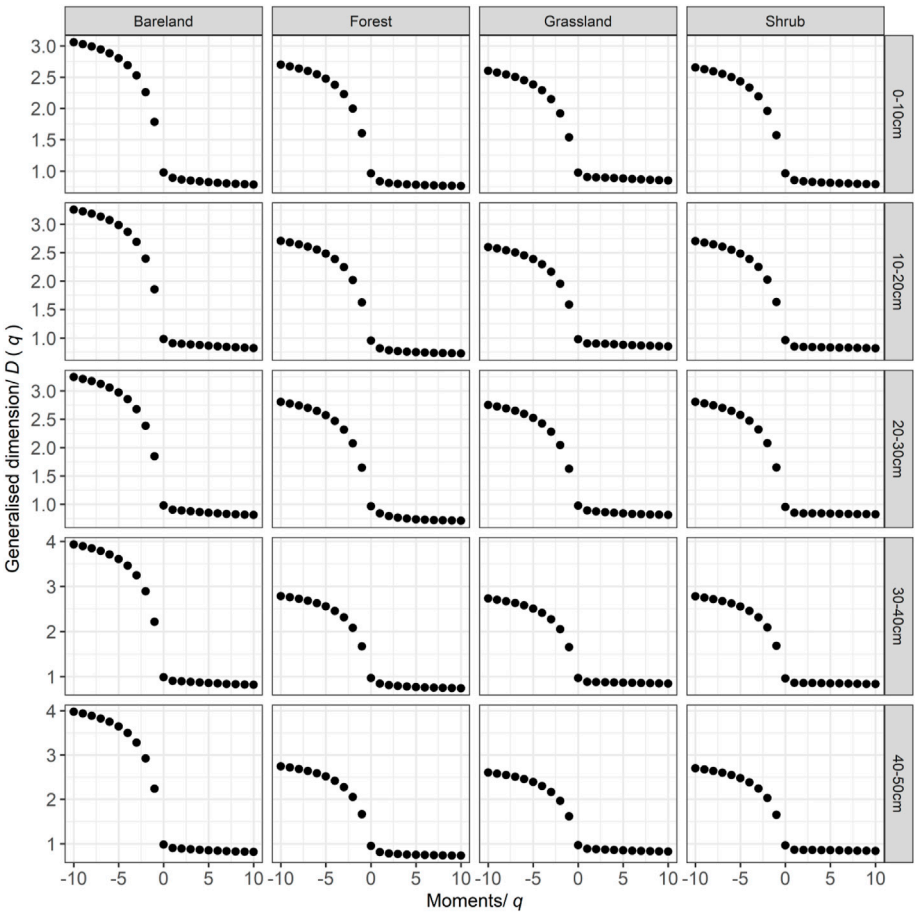

FIGURE 4 | Generalized dimension spectra $D(q)$-q of soil particle-size distribution in different soil layers of four vegetation types in Jiangjiagou Gully.

where $\Delta f[\alpha(q)] < 0$ indicates that the high probability subsets of the soil particle size play the key role in the fractal system, showing a left hook upper convex curve (Tian et al., 2020; Li et al., 2021a).

3.3 Statistical Analysis

A one-way ANOVA in conjunction with the least significant difference (LSD) test ($\alpha = 0.05$) was used to examine sources of variation between soil particles, volumetric fractal dimensions, soil erosion resistance, and multifractal parameters among four vegetation types. Linear regression analysis was conducted to identify the relationships between soil erosion resistance and multifractal parameters. Statistical analyses were performed using R language (Version 3.4.1). All data in all tables are mean ± standard error.

4 RESULTS

4.1 Soil Particle-Size Distribution and Soil Erosion Resistance

The volume fraction distribution of soil showed significant differences across the four vegetation types except very coarse sand, but no significant difference across soil layers (**Table 2**). Among all soil particle-sizes, shrub and forest were characterized by significantly higher silt and clay and lower very fine sand, fine sand, and medium sand, compared with those in bare land and grassland. There was a significant difference in clay between shrub and forest and in coarse sand between bare land and grassland.

Table 2 also summarized the statistics of volumetric fractal dimension and soil erosion resistance across the four vegetation types. The results showed that volumetric fractal dimension was significantly higher in forest and shrub than in bare land and grassland, but there was no significant difference between forest and shrub. Soil erosion resistance showed significant differences of forest > shrub > grassland > bare land.

There was no significant difference among soil layers in volumetric fractal dimension and soil erosion resistance. The interaction between vegetation type and soil layer only markedly influenced soil erosion resistance (**Table 2**).

4.2 Multifractal Characteristics

Rényi dimensions spectra $D(q)$ were calculated for $-10 \le q \le 10$ at 1 lag increment (**Figure 4**). The generalized dimensional spectrum of the soil PSD under different vegetation types across five soil layers decreased monotonically and showed sigmoidal patterns (**Figure 4**). The multifractal parameters following the order of

TABLE 3 | Multifractal parameters among four vegetation types and five soil layers. BL: Bare land; GR: Grassland; SH: Shrub; FO: Forest; D_0: Capacity dimension; D_1: Entropy dimension; D_2: Correlation dimension; α(0): the average value of multifractal singular spectrum; α_{max}: the maximum value of singularity index; α_{min}: the minimum value of singularity index; Δα(q): singularity index; $f(\alpha_{max})$: multifractal spectrum value in α_{max}; $f(\alpha_{min})$: multifractal spectrum value in α_{min}; Δf [α(q)]: the shape of multifractal spectrum. Different letters indicate significant differences at $p < 0.05$. All data are shown using mean ± standard error. * means median; † means mode.

Source	D_0	D_1	D_2	D_1/D_0	α(0)	α_{max}	α_{min}	Δα(*q*)	$f(\alpha_{max})$*1,000	$f(\alpha_{min})$	Δ*f* [α(q)]
Vegetation types (VT)	BL (*n* = 15)0.98 ± 0.01^{a}	0.90 ± 0.01^{a}	0.89 ± 0.02^{a}	0.92 ± 0.01^{a}	1.73 ± 0.05^{a}	3.81 ± 0.43^{a}	0.76 ± 0.03^{a}	3.04 ± 0.41^{a}	0.09 ± 0.16^{b}	0.37 ± 0.09^{b}	-0.37 ± 0.09^{a}
	*0.98 †Null	*0.90 †Null	*0.89 †Null	*0.92 †Null	*1.72 †Null	*3.59 †Null	*0.77 †Null	*2.82 †Null	*0.02 †Null	*0.37 †Null	*–0.37 †Null
	GR (*n* = 15)0.97 ± 0.01^{b}	0.89 ± 0.01^{a}	0.89 ± 0.01^{a}	0.92 ± 0.01^{a}	1.57 ± 0.04^{c}	2.92 ± 0.09^{b}	0.80 ± 0.06^{a}	2.12 ± 0.09^{b}	9.16 ± 12.79^{a}	0.52 ± 0.20^{a}	–0.51 ± 0.20^{b}
	*0.97 †Null	*0.89 †Null	*0.88 †Null	*0.92 †Null	*1.57 †Null	*2.88 †Null	*0.79 †Null	*2.11 †Null	*2.80 †Null	*0.46 †Null	*–0.52 †Null
	SH(*n* = 15)0.96 ± 0.01^{c}	0.86 ± 0.01^{b}	0.85 ± 0.02^{b}	0.89 ± 0.01^{b}	1.62 ± 0.04^{b}	3.00 ± 0.08^{b}	0.80 ± 0.04^{a}	2.20 ± 0.07^{b}	6.13 ± 8.25^{ab}	0.58 ± 0.06^{a}	–0.58 ± 0.06^{b}
	*0.96 †Null	*0.86 †Null	*0.85 †Null	*0.89 †Null	*1.63 †Null	*2.97 †Null	*0.80 †Null	*2.18 †Null	*2.65 †Null	*0.59 †Null	*0.58 †Null
	FO(*n* = 15)0.96 ± 0.01^{c}	0.83 ± 0.02^{c}	0.80 ± 0.02^{c}	0.86 ± 0.01^{c}	1.65 ± 0.06^{b}	3.02 ± 0.07^{b}	0.71 ± 0.05^{b}	2.31 ± 0.09^{b}	0.52 ± 9.42^{ab}	0.49 ± 0.09^{ab}	–0.49 ± 0.09^{ab}
	*0.96 †Null	*0.83 †Null	*0.80 †Null	*0.87 †Null	*1.64 †Null	*3.01 †Null	*0.70 †Null	*2.34 †Null	*–2.00 †Null	*0.51 †Null	*–0.52 †Null
	$p < 0.001$	$p < 0.001$	$p < 0.001$	$p < 0.001$	$p < 0.001$	$p < 0.001$	$p < 0.001$	$p < 0.001$	$p = 0.021$	$p < 0.001$	$p < 0.001$
Soil layers (SL)	0–10 cm (*n* = 12)0.97 ± 0.01^{a}	0.87 ± 0.03^{a}	0.85 ± 0.04^{a}	0.90 ± 0.03^{a}	1.60 ± 0.08^{b}	3.03 ± 0.21^{a}	0.76 ± 0.06^{a}	2.27 ± 0.23^{a}	–2.7 ± 5.71^{b}	0.45 ± 0.13^{a}	–0.46 ± 0.13^{a}
	*0.97 †Null	*0.87 †Null	*0.86 †Null	*0.90 †Null	*1.58 †Null	*2.94 †Null	*0.78 †Null	*2.19 †Null	*0.01 †Null	*0.44 †Null	*-0.46 †Null
	10–20 cm (*n* = 12)0.97 ± 0.01^{a}	0.87 ± 0.04^{a}	0.86 ± 0.05^{a}	0.90 ± 0.03^{a}	1.62 ± 0.07^{ab}	3.10 ± 0.30^{a}	0.77 ± 0.06^{a}	2.33 ± 0.31^{a}	11.47 ± 13.34^{a}	0.47 ± 0.14^{a}	–0.46 ± 0.14^{a}
	*0.97 †Null	*0.88 †Null	*0.87 †Null	*0.90 †Null	*1.60 †Null	*2.97 †Null	*0.79 †Null	*2.20 †Null	*13.48 †Null	*0.47 †Null	*-0.46 †Null
	20–30 cm (*n* = 12)0.97 ± 0.01^{a}	0.87 ± 0.03^{a}	0.85 ± 0.04^{a}	0.90 ± 0.02^{a}	1.62 ± 0.05^{ab}	3.19 ± 0.23^{a}	0.76 ± 0.06^{a}	2.43 ± 0.23^{a}	-0.26 ± 3.53^{b}	0.49 ± 0.12^{a}	0.49 ± 0.12^{a}
	*0.97 †Null	*0.88 †Null	*0.87 †Null	*0.91 †Null	*1.62 †Null	*3.10 †Null	*0.77 †Null	*2.34 †Null	*0.98 †Null	*0.53 †Null	*-0.54 †Null
	30–40 cm (*n* = 12)0.97 ± 0.01^{a}	0.87 ± 0.02^{a}	0.86 ± 0.03^{a}	0.90 ± 0.02^{a}	1.67 ± 0.06^{ab}	3.27 ± 0.52^{a}	0.78 ± 0.06^{a}	2.49 ± 0.53^{a}	10.86 ± 9.23^{a}	0.52 ± 0.17^{a}	-0.51 ± 0.17^{a}
	*0.97 †Null	*0.87 †Null	*0.87 †Null	*0.90 †Null	*1.64 †Null	*3.08 †Null	*0.78 †Null	*2.27 †Null	*13.50 †Null	*0.54 †Null	*-0.54 †Null
	40–50 cm (*n* = 12)0.97 ± 0.01^{a}	0.87 ± 0.04^{a}	0.85 ± 0.04^{a}	0.90 ± 0.03^{a}	1.69 ± 0.07^{a}	3.31 ± 0.65^{a}	0.77 ± 0.05^{a}	2.54 ± 0.05^{a}	1.41 ± 1.40^{b}	0.52 ± 0.16^{b}	-0.52 ± 0.16^{b}
	*0.97 †Null	*0.87 †Null	*0.87 †Null	*0.90 †Null	*1.67 †Null	*3.00 †Null	*0.77 †Null	*2.22 †Null	*1.83 †Null	*0.53 †Null	*-0.53 †Null
	$p = 0.789$	$p = 0.987$	$p = 0.993$	$p = 0.999$	$p = 0.008$	$p = 0.452$	$p = 0.941$	$p = 0.505$	$p < 0.001$	$p = 0.738$	$p = 0.760$
VT×SL	$p = 0.090$	$p = 0.007$	$p = 0.081$	$p = 0.263$	$p = 0.679$	$p < 0.001$	$p = 0.943$	$p < 0.001$	$p = 0.096$	$p = 0.970$	$p = 0.973$

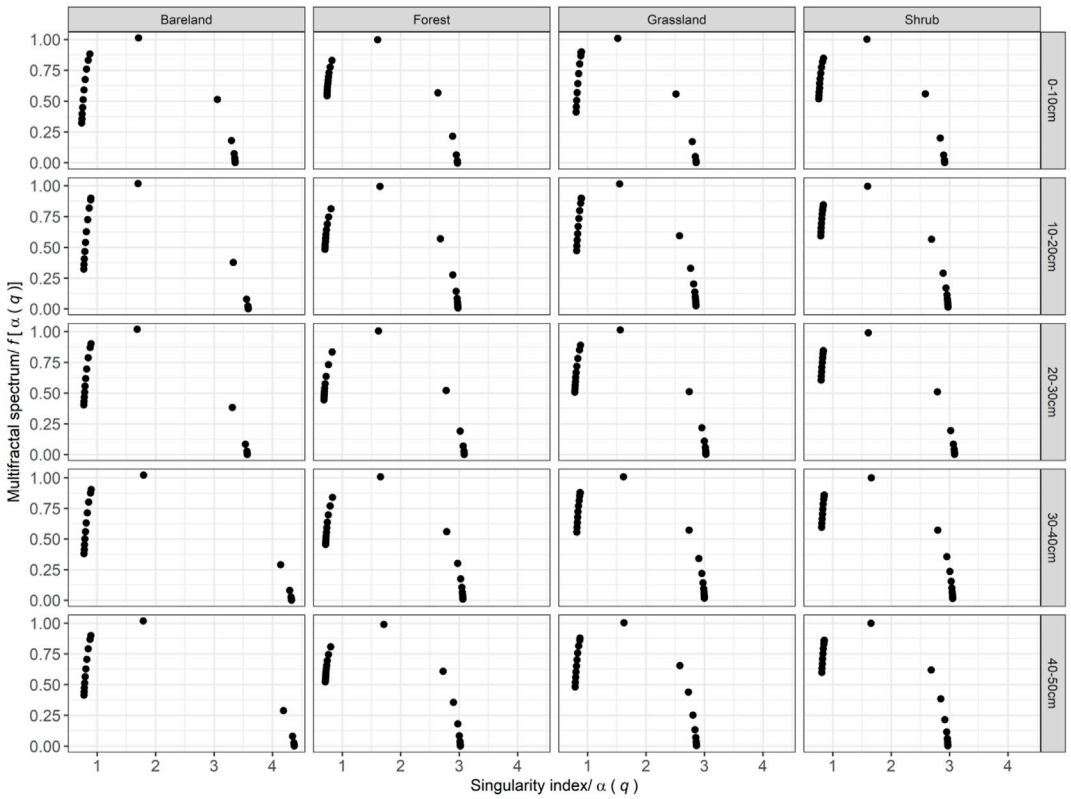

FIGURE 5 | Multifractal spectrum functions of the soil particle-size distribution in different soil layers of four vegetation types in Jiangjiagou Gully.

capacity dimension (D_0) > entropy dimension (D_1) > correlation dimension (D_2) for each vegetation type showed the non-uniformity of the soil PSD, indicating more pronounced non-uniformity in sparse areas than in dense areas (Li et al., 2021b).

Generally, multifractal parameters are higher in bare land than in the other vegetation types (**Table 3**) except for α_{min}, $f(\alpha_{max})$, and $f(\alpha_{min})$, indicating that the soil PSD in bare land has a wider range or more homogeneous distribution in particle size and a higher heterogeneity. D_0, D_1, and D_2 were highest in grassland, intermediate in shrub, and lowest in forest. D_1/D_0 was highest in bare land and grassland, intermediate in shrub, and lowest in forest, whereas α_0 was higher in shrub and forest than in grassland. There were no significant differences in α_{max}, $\Delta\alpha$, $f(\alpha_{max})$, and $f(\alpha_{min})$ across grassland, shrub, and forest, whereas α_{min} was lower in forest than in the other vegetation types.

There was no significant difference among soil layers in multifractal parameters. The interaction between vegetation type and soil layer only has significant effects on D_1, α_{max}, and $\Delta\alpha$ (**Table 3**).

4.3 Multifractal Singularity Spectrum

The multifractal singularity spectra named $\Delta f[\alpha(q)]$-$\alpha(q)$ curves of all vegetation types across five soil layers are asymmetric, left hook upper, and convex functions (**Figure 5**), indicating that the soil PSD has heterogeneous and multifractal characteristics. In the right part of all curves, the slope downward to the right are higher in bare land than in the other vegetation types across five soil layers, suggesting that bare land experiencing heavy soil erosion had a higher superposition of soil particle size. Therefore, the local average singularity ($\alpha(0)$), the width of the multifractal singularity spectrum ($\Delta\alpha(q)$), and the symmetry degree of the multifractal spectrum ($\Delta f[\alpha(q)]$) were significantly higher in bare land than the other vegetation types (**Table 3**).

4.4 Relationships Between Multifractal Parameters and Soil Erosion Resistance

Linear regression analysis was conducted between soil erosion resistance and multifractal parameters (D, D_0, D_1, D_2, D_1/D_0, $\alpha(0)$, $\Delta\alpha(q)$, $\Delta f[\alpha(q)]$) in four vegetation types across five soil layers (**Figure 6**). We found that soil erosion resistance was significantly negatively correlated with D_0, D_1, D_2, $\alpha(0)$, $\Delta\alpha(q)$, $\Delta f[\alpha(q)]$ but positively with D and D_1/D_0, indicating that multifractal parameters could represent the ability of vegetation types for soil erosion control to a certain extent.

5 DISCUSSION

5.1 Soil Size Distribution, Volumetric Fractal Dimension, and Soil Erosion Resistance in Different Vegetation Types

Vegetation types can effectively control soil particle size distribution (Gui et al., 2011). Our study proved it that shrub

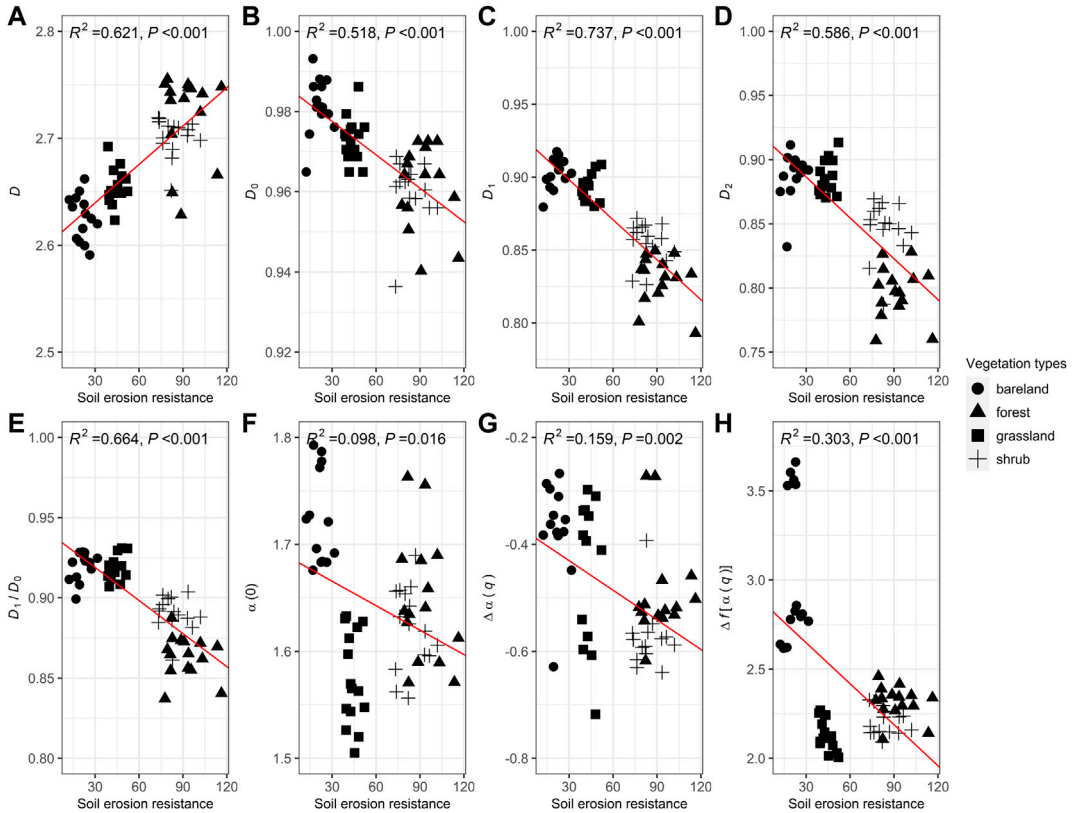

FIGURE 6 | Relationships between soil erosion resistance and multifractal parameters including D**(A)**, D_0**(B)**, D_1**(C)**, D_2**(D)**, D_1/D_0**(E)**, α(0) **(F)**, Δα(q) **(G)**, Δf [α(q)]**(H)**.

and forest had significantly higher volume fractions of clay and silt but lower volume fractions of very fine sand, fine sand, medium sand, and coarse sand compared with bare land and grassland, indicating that vegetation with complicated community structure, higher vegetation coverage, and greater species number could improve the soil structure (Liu et al., 2017). In other words, fine particles are easily eroded and detached from surface soil due to stronger soil erosion in younger vegetation communities, such as bare land and grassland. This result is consistent with the findings of Burylo et al. (2012), who suggest that fine particles would be preferentially detached, while coarse particles would be deposited first during water erosion. It has been well documented that soil particle size distribution can affect the structure and properties of soil (Lyu et al., 2015; Ding and Huang, 2017). Volumetric fractal dimension (D) ranging from 2.63 to 2.72 in our study sites is similar to the findings of Peng et al. (2014), who observed that the D value of forest ranged from 2.50 to 2.68. Previous studies also demonstrated that soils had good texture when D values range from 2.60 to 2.80 (Liu et al., 2009; Xu et al., 2013). However, this strategy may not be working in our case, because soils in our study developed from landslide mass (Lin et al., 2019). This may be due to discrepancies in soil formation background, parent material, and development process between our study sites and the other sites.

It is well-known that the effects of vegetation on soil erosion control can increase in accordance with positive community succession (Lin et al., 2014; Cui et al., 2019). Although our study does not carry out long-term field observations on the process of vegetation succession, it does reveal that soil erosion resistance will fluctuate in different vegetation types. For example, we observed that the community structure, vegetation coverage, and species number increased in order of forest > shrub > grassland > bare land correspondingly; the mean soil erosion resistance is in order of forest > shrub > grassland > bare land. This result is consistent with previous investigations, which highlighted species composition and community structure as the indicators of soil and water conservation (Wang and Liu, 1999; Ma and Jiao, 2005).

However, soil layer did not significantly affect any concerned parameters, indicating that short-term (<40 years) vegetation succession could not change soil properties in soil depth (Zhou et al., 2009).

5.2 Multifractal Features in Different Vegetation Types

Multifractal analysis can capture the inner variations in the soil PSD and the inhomogeneity of its fractal structure using a distributional spectrum (Miranda et al., 2006; Cui et al., 2019; Li et al., 2021b). Capacity dimension (D_0), entropy dimension (D_1), correlation dimension (D_2), and D_1/D_0 could be used to describe the ranges of continuous distribution and particle size distribution, the homogeneity and heterogeneity among fractions, respectively

(Montero, 2005; Miranda et al., 2006). In this study, all soils in four vegetation types across 5layers showed the trend of $D_0 > D_1 > D_2$, indicating that soils have high-dispersion particle distribution in a disordered system. This result is consistent with the findings of Cui et al. (2019), who observed that trapped sediment similar to the soil in our study displayed such laws.

Bare land and grassland had higher D_1/D_0 values than shrub and forest, suggesting that measures dispersed over the set of sizes in their soils, because D_1/D_0 value close to 1 will indicate sets with similar dimensions (Wang et al., 2008). Similarly, $\alpha(0)$, $\Delta\alpha(q)$, and $\Delta f\ [\alpha(q)]$ are significantly higher in bare land than in the other vegetation types, indicating that there was a wider range of variability in the heterogeneity of the samples collected from bare land. Therefore, the $\Delta f\ [\alpha(q)]$-$\alpha(q)$ curve of bare land across five soil layers is more asymmetric and has a higher slope downward to the right in its right part than the other vegetation types. Therefore, the bare land has a higher superposition of soil particle size. This result is consistent with other studies demonstrating significantly negative impacts of bare land on soil particle size distribution (Cui et al., 2005; Luo et al., 2019).

5.3 Influence of Multifractal Parameters on Soil Erosion Resistance

Soil erosion resistance in all four vegetation types across five soil layers exhibit significant linear correlations with D, D_0, D_1, D_2, D_1/D_0, $\alpha(0)$, $\Delta\alpha(q)$, and $\Delta f\ [\alpha(q)]$. It implies that multifractal parameters could represent the ability of soil erosion control by vegetation. However, $\alpha(0)$ and $\Delta\alpha(q)$ are less strongly related with soil erosion resistance than the other six multifractal parameters. In other words, $\alpha(0)$ and $\Delta\alpha(q)$ were not suitable for predicting soil erosion resistance, but the other six multifractal parameters can reveal erosion control effects and determine ecosystem service value of vegetation in eroded lands by considering their capacity for soil erosion resistance, because erosion control of vegetation is listed as one of the 17 major ecosystem services (Costanza et al., 1997). However, this statement should be tempered by the fact that the experiments cannot carry out on-site field observations on the whole process of vegetation succession from bare land to forest. Elucidating the relationships between soil erosion resistance and vegetation types in different soil depths would require additional research.

6 CONCLUSION

In this study, we analyzed the differences in soil particle size distribution, soil erosion resistance and multifractal parameters among four vegetation types (bare land, grassland, shrub, and forest) across five layers (0–10 cm, 10–20 cm, 20–30 cm, 30–40 cm, and 40–50 cm). Our results suggest that vegetation types significantly affect soil particle size distribution, soil erosion resistance, and multifractal parameters. The generalized dimensions spectra curves of the PSD in four vegetation types across five soil layers are all sigmoidal, whereas the singular spectrum function shows an asymmetric upward convex curve. Despite some limitations, this study provided an important insight for the evaluation of soil structure improvement and the effects of erosion control by vegetation restoration in dry-hot valley area. Future research should extend this work by carrying out long-term on-site field observations to determine the change process of soil properties during vegetation succession.

DATA AVAILABILITY STATEMENT

The original contributions presented in the study are included in the article/Supplementary Material, further inquiries can be directed to the corresponding author.

AUTHOR CONTRIBUTIONS

SL and RG contributed equally to this work and should be considered co-first authors. SL, RG, and YL contributed to the conception and design of the study, submission preparation, and idea discussion. MH, LY, and HY carried out field work and determined soil particle size distribution. SL, RG, CY, and XT performed the statistical analysis. SL, RG, and YL wrote the first draft of the manuscript. JL, and YL contributed to manuscript revision, read, and approved the submitted version.

FUNDING

This work was supported by the joint funds of the Fujian Provincial Natural Science Foundation (Grant No. 2021J01060), the National Natural Science Foundation of China (No. 42071132 and 41790434), and the Key Laboratory of Mountain Hazards and Surface Process, Chinese Academy of Sciences (No. 2019).

ACKNOWLEDGMENTS

We thank Ying Liu, Jingwen He, Yu Cui, and Jianzhao Wu for help collecting the data.

REFERENCES

Asadi, H., Moussavi, A., Ghadiri, H., and Rose, C. W. (2011). Flow-driven Soil Erosion Processes and the Size Selectivity of Sediment. *J. Hydrology* 406, 73–81. doi:10.1016/j.jhydrol.2011.06.010

Bieganowski, A., Chojecki, T., Ryżak, M., Sochan, A., and Lamorski, K. (2013). Methodological Aspects of Fractal Dimension Estimation on the Basis of Particle Size Distribution. *Vadose Zone J.* 12 (1), vzj20120064–9. doi:10.2136/vzj2012.0064

Biswas, A. (2019). Joint Multifractal Analysis for Three Variables: Characterizing the Effect of Topography and Soil Texture on Soil Water Storage. *Geoderma* 334, 15–23. doi:10.1016/j.geoderma.2018.07.035

Bochet, E., Poesen, J., and Rubio, J. L. (2000). Mound Development as an Interaction of Individual Plants with Soil, Water Erosion and Sedimentation

Processes on Slopes. *Earth Surf. Process. Landforms* 25, 847–867. doi:10.1002/1096-9837(200008)25:8<847::aid-esp103>3.0.co;2-q

Burylo, M., Rey, F., Bochet, E., and Dutoit, T. (2012). Plant Functional Traits and Species Ability for Sediment Retention during Concentrated Flow Erosion. *Plant Soil* 353, 135–144. doi:10.1007/s11104-011-1017-2

Chen, A. M., Deng, H. J., Yan, S. W., Lin, Y. M., Zhang, G. S., and Du, K. (2016). Fractal Features of Soil and Their Relation with Soil Fertility under Five Vegetation in Jiangjiagou Gully. *Mt. Res.* 34 (3), 290–296. doi:10.16089/j.cnki.1008-2786.000130

Chen, S., Wang, D. J., Mei, Y. L., Chen, X. Y., and Zhang, S. J. (2014). The Research of Grain Composition and Sediment Generation on Landslip-Collapse Soil in Debris Flow Original Area. *Mt. Res.* 32 (1), 66–73. doi:10.16089/j.cnki.1008-2786.2014.01.009

Costanza, R., d'Arge, R., de Groot, R., Farber, S., Grasso, M., Hannon, B., et al. (1997). The Value of the World's Ecosystem Services and Natural Capital. *Nature* 387, 253–260. doi:10.1016/S0921-8009(98)00020-210.1038/387253a0

Cui, P., Wang, D. J., and Wei, F. Q. (2005). Model and Effect of Ecological Restoration of Dry-Hot Valley: A Case Study of the CAS Dongchuan Debris Flow Observation Station. *Sci. Soil Water Conserv.* 3, 60–64. doi:10.16843/j.sswc.2005.03.012

Cui, Y., Li, J., Chen, A., Wu, J., Luo, Q., Rafay, L., et al. (2019). Fractal Dimensions of Trapped Sediment Particle Size Distribution Can Reveal Sediment Retention Ability of Common Plants in a Dry-Hot Valley. *Catena* 180, 252–262. doi:10.1016/j.catena.2019.04.031

Dai, Z., Ma, C., Miao, L., Li, M., Wu, J., and Wang, X. (2022). Initiation Conditions of Shallow Landslides in Two Man-Made Forests and Back Estimation of the Possible Rainfall Threshold. *Landslides* 19, 1031–1044. doi:10.1007/s10346-021-01823-1

De Wang, D., Fu, B., Zhao, W., Hu, H., and Wang, Y. (2008). Multifractal Characteristics of Soil Particle Size Distribution under Different Land-Use Types on the Loess Plateau, China. *Catena* 72, 29–36. doi:10.1016/j.catena.2007.03.019

Deng, H. J., Zhang, G. S., Yu, W., Wu, C. Z., Hong, W., and Lin, Y. M. (2015). Change in Basic Characters and Fractal Dimension of Soil in Destroyed Vegetation Management Region after Earthquake and Their Correlation Analysis. *J. Plant Resour. Environ.* 24 (1), 12–18. doi:10.3969/j.issn.1674-7895.2015.01.02

Deng, J., Ma, C., and Zhang, Y. (2022). Shallow Landslide Characteristics and its Response to Vegetation by Example of July 2013, Extreme Rainstorm, Central Loess Plateau, China. *Bull. Eng. Geol. Environ.* 81 (3), 1–18. doi:10.1007/s10064-022-02606-1

Descheemaeker, K., Nyssen, J., Rossi, J., Poesen, J., Haile, M., Raes, D., et al. (2006). Sediment Deposition and Pedogenesis in Exclosures in the Tigray Highlands, Ethiopia. *Geoderma* 132, 291–314. doi:10.1016/j.geoderma.2005.04.027

Ding, W., and Huang, C. (2017). Effects of Soil Surface Roughness on Interrill Erosion Processes and Sediment Particle Size Distribution. *Geomorphology* 295, 801–810. doi:10.1016/j.geomorph.2017.08.033

Guan, X. Y., Yang, P. L., and Lv, Y. (2011). Analysis on Spatial Variability of Soil Properties Based on Multifractal Theory. *J. Basic Sci. Eng.* 19 (5), 712–720. doi:10.3969/j.issn.1005-0930.2011.05.003

Gui, D. W., Lei, J. Q., Zeng, F. J., Mu, G. J., and Li, K. F. (2011). Characteristics of Soil Particle Size Distribution in Different Land-Use Types of Oasis Rim. *Sci. Silvae Sin.* 47 (1), 22–28. doi:10.3969/j.issn.1005-6327.2002.06.007

Gyssels, G., Poesen, J., Bochet, E., and Li, Y. (2005). Impact of Plant Roots on the Resistance of Soils to Erosion by Water: A Review. *Prog. Phys. Geog.* 29, 189–217. doi:10.1191/0309133305pp443ra

Jin, X., and Chen, L. H. (2019). Soil Anti-scouribility and Surface Root Distribution of Different Vegetation Types in Loess Region of Western Shanxi Province. *Chin. J. Soil Water Conserv.* 33 (6), 120–126. doi:10.13870/j.cnki.stbcxb.2019.06.017

Li, J.-l., Bao, Y.-h., Wei, J., He, X.-b., Tang, Q., and Nambajimana, J. d. D. (2019). Fractal Characterization of Sediment Particle Size Distribution in the Water-Level Fluctuation Zone of the Three Gorges Reservoir, China. *J. Mt. Sci.* 16, 2028–2038. doi:10.1007/s11629-019-5456-1

Li, J., He, X., Wei, J., Bao, Y., Tang, Q., Nambajimana, J. d. D., et al. (2021b). Multifractal Features of the Particle-Size Distribution of Suspended Sediment in the Three Gorges Reservoir, China. *Int. J. Sediment Res.* 36, 489–500. doi:10.1016/j.ijsrc.2020.12.003

Li, J., Liu, Y., Wu, J., He, J. W., He, J., Cui, Y., et al. (2021a). Plant Morphological and Functional Characteristics Combined with Elevation and Aspect Influence Phytogenic Mound Parameters in a Dry-Hot Valley. *J. Soil Water Conserv.* 76 (2), 142–152. doi:10.2489/jswc.2021.00031

Li, S.-y., Lin, J.-y., Pan, J.-h., Yu, H., Gao, R.-y., and Yang, L.-s. (2021c). Multifractal Characteristics of Soil Particle-Size Distribution Under Different Land-Use Types in an Area with High Frequency Debris Flow. *Chin. J. Appl. Environ. Biol.* 27 (4), 893–900. doi:10.19675/j.cnki.1006-687x.2020.11046

Lin, Y.-m., Cui, P., Ge, Y.-g., Chen, C., Wang, D.-j., Wu, C.-z., et al. (2014). The Succession Characteristics of Soil Erosion during Different Vegetation Succession Stages in Dry-Hot River Valley of Jinsha River, Upper Reaches of Yangtze River. *Ecol. Eng.* 62, 13–26. doi:10.1016/j.ecoleng.2013.10.020

Lin, Y., Chen, A., Yan, S., Rafay, L., Du, K., Wang, D., et al. (2019). Available Soil Nutrients and Water Content Affect Leaf Nutrient Concentrations and Stoichiometry at Different Ages of *Leucaena Leucocephala* Forests in Dry-Hot Valley. *J. Soils Sediments* 19, 511–521. doi:10.1007/s11368-018-2029-9

Liu, L., Liu, Y., Hui, R., and Xie, M. (2017). Recovery of Microbial Community Structure of Biological Soil Crusts in Successional Stages of Shapotou Desert Revegetation, Northwest China. *Soil Biol. Biochem.* 107, 125–128. doi:10.1016/j.soilbio.2016.12.030

Liu, X., Zhang, G., Heathman, G. C., Wang, Y., and Huang, C.-h. (2009). Fractal Features of Soil Particle-Size Distribution as Affected by Plant Communities in the Forested Region of Mountain Yimeng, China. *Geoderma* 154, 123–130. doi:10.1016/j.geoderma.2009.10.005

Liu, X., Zhang, G., Heathman, G. C., Wang, Y., and Huang, C.-h. (2009). Fractal Features of Soil Particle-Size Distribution as Affected by Plant Communities in the Forested Region of Mountain Yimeng, China. *Geoderma* 154, 123–130. doi:10.1016/j.geoderma.2009.10.005

Liu, Z., Qiu, H., Ma, S., Yang, D., Pei, Y., Du, C., et al. (2021). Surface Displacement and Topographic Change Analysis of the Changhe Landslide on September 14, 2019, China. *Landslides* 18 (4), 1471–1483. doi:10.1007/s10346-021-01626-4

Liu, Y., Qiu, H., Yang, D., Liu, Z., Ma, S., Pei, Y., et al. (2022). Deformation Responses of Landslides to Seasonal Rainfall Based on InSAR and Wavelet Analysis. *Landslides* 19, 199–210. doi:10.1007/s10346-021-01785-4

Luo, Q. H., Wu, J. Z., Cui, Y., Sun, F., Lin, Y. M., Wang, D. J., et al. (2019). Characteristics of Soil Properties and Fractal Dimensions of Destroyed and Naturally Restored Forest Land under Flood Disaster Disturbance. *Chin. J. Appl. Environ. Biol.* 25 (1), 29–37. doi:10.19675/j.cnki.1006-687x.2018.04032

Lyu, X., Yu, J., Zhou, M., Ma, B., Wang, G., Zhan, C., et al. (2015). Changes of Soil Particle Size Distribution in Tidal Flats in the Yellow River Delta. *PLoS One* 10 (3), e0121368. doi:10.1371/journal.pone.0121368

Ma, C., Wang, Y.-j., Du, C., Wang, Y.-q., and Li, Y.-p. (2016). Variation in Initiation Condition of Debris Flows in the Mountain Regions Surrounding Beijing. *Geomorphology* 273, 323–334. doi:10.1016/j.geomorph.2016.08.027

Ma, S., Qiu, H., Hu, S., Yang, D., and Liu, Z. (2021). Characteristics and Geomorphology Change Detection Analysis of the Jiangdingya Landslide on July 12, 2018, China. *Landslides* 18, 383–396. doi:10.1007/s10346-020-01530-3

Ma, X. H., and Jiao, J. Y. (2005). Characteristics of Vegetation with Natural Restoration in Removal Lands in Loess Hilly-Gully Region and the Relationship between the Characteristics and Soil Environment. *Sci. Soil Water Conserv.* 3 (2), 15–22. doi:10.3969/j.issn.1672-3007.2005.02.004

McVicar, T. R., Van Niel, T. G., Li, L., Wen, Z., Yang, Q., Li, R., et al. (2010). Parsimoniously Modelling Perennial Vegetation Suitability and Identifying Priority Areas to Support China's Re-vegetation Program in the Loess Plateau: Matching Model Complexity to Data Availability. *For. Ecol. Manag.* 259, 1277–1290. doi:10.1016/j.foreco.2009.05.002

Miranda, J. G. V., Montero, E., Alves, M. C., Paz González, A., and Vidal Vázquez, E. (2006). Multifractal Characterization of Saprolite Particle-Size Distributions after Topsoil Removal. *Geoderma* 134, 373–385. doi:10.1016/j.geoderma.2006.03.014

Montero, E. (2005). Rényi Dimensions Analysis of Soil Particle-Size Distributions. *Ecol. Model.* 182, 305–315. doi:10.1016/j.ecolmodel.2004.04.007

Peng, G., Xiang, N., Lv, S.-q., and Zhang, G.-c. (2014). Fractal Characterization of Soil Particle-Size Distribution under Different Land-Use Patterns in the Yellow River Delta Wetland in China. *J. Soils Sediments* 14 (6), 1116–1122. doi:10.1007/s11368-014-0876-6

Perfect, E., and Kay, B. D. (1995). Applications of Fractals in Soil and Tillage Research: A Review. *Soil Tillage Res.* 36, 1–20. doi:10.1016/0167-1987(96)81397-3

Podwojewski, P., Janeau, J. L., Grellier, S., Valentin, C., Lorentz, S., and Chaplot, V. (2011). Influence of Grass Soil Cover on Water Runoff and Soil Detachment under Rainfall Simulation in a Sub-humid South African Degraded Rangeland. *Earth Surf. Process. Landforms* 36, 911–922. doi:10.1002/esp.2121

Rodríguez-Lado, L., and Lado, M. (2017). Relation between Soil Forming Factors and Scaling Properties of Particle Size Distributions Derived from Multifractal Analysis in Topsoils from Galicia (NW Spain). *Geoderma* 287, 147–156. doi:10.1016/j.geoderma.2016.08.005

Schillereff, D. N., Chiverrell, R. C., Macdonald, N., and Hooke, J. M. (2014). Flood Stratigraphies in Lake Sediments: A Review. *Earth-Science Rev.* 135, 17–37. doi:10.1016/j.earscirev.2014.03.011

Shi, Z. H., Fang, N. F., Wu, F. Z., Wang, L., Yue, B. J., and Wu, G. L. (2012). Soil Erosion Processes and Sediment Sorting Associated with Transport Mechanisms on Steep Slopes. *J. Hydrology* 454-455, 123–130. doi:10.1016/j.jhydrol.2012.06.004

Su, Y. Z., Zhao, H. L., Zhao, W. Z., and Zhang, T. H. (2004). Fractal Features of Soil Particle Size Distribution and the Implication for Indicating Desertification. *Geoderma* 122, 43–49. doi:10.1016/j.geoderma.2003.12.003

Tian, X. F., Su, F. H., Guo, X. J., Liu, J. J., and Li, Y. (2020). Material Sources Supplying Debris Flows in Jiangjia Gully. *Environ. Earth Sci.* 79 (13), 1–20. doi:10.1007/s12665-020-09020-4

Tyler, S. W., and Wheatcraft, S. W. (1992). Fractal Scaling of Soil Particle-Size Distributions: Analysis and Limitations. *Soil Sci. Soc. Am. J.* 56 (2), 362–369. doi:10.2136/sssaj1992.03615995005600020005x

Wang, D. J., Cui, P., Zhu, B., and Wang, Y. K. (2004). Vegetation Rehabilitation Techniques and Ecological Effects in Dry-Hot Valley of Jinsha River. *J. Soil Water Conserv.* 18 (5), 95–98. doi:10.13870/j.cnki.stbcxb.2004.05.024

Wang, G. L., Zhou, S. L., and Zhao, Q. G. (2005). Volume Fractal Dimension of Soil Particles and its Applications to Land Use. *Acta Pedol. Sin.* 42 (4), 545–550. doi:10.3321/j.issn:0564-3929.2005.04.003

Wang, H. S., and Liu, G. S. (1999). Analyses on Vegetation Structures and Their Controlling Soil Erosion. *J. Arid. Land Resour. Environ.* 13 (2), 62–68.

Wang, J., Zhang, J., and Feng, Y. (2019). Characterizing the Spatial Variability of Soil Particle Size Distribution in an Underground Coal Mining Area: An Approach Combining Multi-Fractal Theory and Geostatistics. *Catena* 176, 94–103. doi:10.1016/j.catena.2019.01.011

Wei, X.-l., Chen, N.-s., Cheng, Q.-g., He, N., Deng, M.-f., and Tanoli, J. I. (2014). Long-term Activity of Earthquake-Induced Landslides: A Case Study from Qionghai Lake Basin, Southwest of China. *J. Mt. Sci.* 11, 607–624. doi:10.1007/s11629-013-2970-4

Xie, X. J., and Wei, F. Q. (2011). Characteristics of Soil Particle Fractal Dimension under Different Coverage Grassland of the Area with High-Frequency Debris Flow. *J. Soil Water Conserv.* 25 (4), 202–206. doi:10.13870/j.cnki.stbcxb.2011.04.053

Xu, G., Li, Z., and Li, P. (2013). Fractal Features of Soil Particle-Size Distribution and Total Soil Nitrogen Distribution in a Typical Watershed in the Source Area of the Middle Dan River, China. *Catena* 101, 17–23. doi:10.1016/j.catena.2012.09.013

Xu, W. X., Bao, Y. H., Wei, J., Yang, L., He, X. B., and Li, J. L. (2019). Effects of Typical Herbaceous Roots on Soil Scour Resistance in Water-Level-Fluctuation Zone of Reservoir. *Chin. J. Soil Water Conserv.* 33 (4), 65–71+109. doi:10.13870/j.cnki.stbcxb.2019.04.010

Yang, D., Qiu, H., Ma, S., Liu, Z., Du, C., Zhu, Y., et al. (2022). Slow Surface Subsidence and its Impact on Shallow Loess Landslides in a Coal Mining Area. *Catena* 209, 105830. doi:10.1016/j.catena.2021.105830

Zhang, J. R., Wang, J. M., Zhu, Y. C., Li, B., and Wang, P. (2017). Application of Fractal Theory on Pedology: a Review. *Chin. J. Soil Sci.* 48 (1), 221–228. doi:10.19336/j.cnki.trtb.2017.01.29

Zhang, P., Yao, W., Liu, G., Xiao, P., and Sun, W. (2020). Experimental Study of Sediment Transport Processes and Size Selectivity of Eroded Sediment on Steep Pisha Sandstone Slopes. *Geomorphology* 363, 107211. doi:10.1016/j.geomorph.2020.107211

Zhou, X. F., Zhao, R., Li, Y. Y., and Chen, X. Y. (2009). Effects of Land Use Types on Particle Size Distribution of Reclaimed Alluvial Soils of the Yangtze Estuary. *Acta Ecol. Sin.* 29 (10), 5544–5551. doi:10.3321/j.issn:1000-0933.2009.10.044

Zhou, W., Qiu, H., Wang, L., Pei, Y., Tang, B., Ma, S., et al. (2022). Combining Rainfall-Induced Shallow Landslides and Subsequent Debris Flows for Hazard Chain Prediction. *Catena* 213, 106199. doi:10.1016/j.catena.2022.106199

Conflict of Interest: The authors declare that the research was conducted in the absence of any commercial or financial relationships that could be construed as a potential conflict of interest.

Publisher's Note: All claims expressed in this article are solely those of the authors and do not necessarily represent those of their affiliated organizations, or those of the publisher, the editors and the reviewers. Any product that may be evaluated in this article, or claim that may be made by its manufacturer, is not guaranteed or endorsed by the publisher.